Available online at www.sciencedirect.com
ScienceDirect
International Journal of Solids and Structures 44 (2007) 1–17
INTERNATIONAL JOURNAL OF SOLIDS and STRUCTURES
www.elsevier.com/locate/ijsolstr

Analysis of spherical indentation of superelastic shape memory alloys

Wenyi Yan [a,*], Qingping Sun [b], Xi-Qiao Feng [c], Linmao Qian [d]

[a] School of Engineering and Information Technology, Deakin University, Geelong, Victoria 3217, Australia
[b] Department of Mechanical Engineering, The Hong Kong University of Science and Technology, Hong Kong, China
[c] Department of Engineering Mechanics, Tsinghua University, Beijing 100084, China
[d] Tribology Research Institute, National Traction Power Laboratory, Southwest Jiaotong University, Chengdu 610031, Sichuan Province, China

Received 14 June 2005; received in revised form 4 April 2006
Available online 20 April 2006

Abstract

Dimensional analysis and the finite element method are applied in this paper to study spherical indentation of superelastic shape memory alloys. The scaling relationships derived from dimensional analysis bridge the indentation response and the mechanical properties of a superelastic shape memory alloy. Several key variables of a superelastic indentation curve are revealed and examined. We prove that the bifurcation force in a superelastic indentation curve only relies on the forward transformation stress and the elastic properties of the initial austenite; and the return force in a superelastic indentation curve only relies on the reverse transformation stress and the elastic properties of the initial austenite. Furthermore, the dimensionless functions to determine the bifurcation force and the return force are proved to be identical. These results not only enhance our understanding of spherical indentation of superelastic shape memory alloys, but also provide the theoretical basis for developing a practicable method to calibrate the mechanical properties of a superelastic material from the spherical indentation test.
© 2006 Elsevier Ltd. All rights reserved.

Keywords: Shape memory alloys; Superelasticity; Spherical indentation; Transformation stress; Hardness; Finite element simulations

1. Introduction

Shape memory alloys (SMAs), represented by NiTi, are well known for their extraordinary shape memory and superelastic properties. These properties are due to the intrinsic thermoelastic martensitic transformation under thermal or mechanical loading conditions at different temperatures. At a relatively low temperature and under an external force, the initial parent phase (austenite) can transform into a martensite phase accompanied by macroscopic deformation. Upon unloading to zero, the material remains in a martensite state with

* Corresponding author. Tel.: +61 35 22 72 082; fax: +61 35 22 72 167.
E-mail address: wenyi.yan@deakin.edu.au (W. Yan).

0020-7683/$ - see front matter © 2006 Elsevier Ltd. All rights reserved.
doi:10.1016/j.ijsolstr.2006.04.007

residual strain. Then, when the material is heated to a certain temperature, the martensite can transform back to the initial austenite phase with the material returning to its initial shape. This is the shape memory effect. For the same material, when loaded at a higher temperature, the transformed martensite due to loading can transform back to austenite during unloading while recovering a large amount of the prior deformation. This extraordinary recoverable deformation behavior is called superelasticity or pseudoelasticity.

Both the shape memory effect and superelastic deformation have been exploited to design SMA-based functional and smart structures. One of the most successful application fields is biomedical engineering with the famous example of NiTi vascular stents to reinforce blood vessels by applying either shape memory behavior or superelastic mechanisms. Recently, SMA thin films have been recognized as a promising and high performance material in the field of micro-electro-mechanical system (MEMS). Since SMA thin films are much easier to heat or cool than bulk samples, the response time can be reduced substantially and therefore the speed of operation could be increased significantly. The main advantages of NiTi thin film include high power density, large displacement and actuation force, low operation voltage, etc., and it is considered as a core technology for actuation of some MEMS devices and in extreme environments, such as radioactive, space, biological and corrosive conditions (Fu et al., 2004).

The reversible phase transformation in SMA not only demonstrates the shape memory effect and superelastic behavior but also signals extraordinary mechanical properties. In recent years, the superior wear-resistance of superelastic NiTi SMA has attracted much attention. For examples, Richman et al. (1995) discovered that NiTi alloys are much more resistant to cavitation erosion than even the best stainless steels. Jin and Wang (1988) revealed that the sliding wear-resistance of NiTi is better than that of nitrided 38CrMoA1A alloy steel. Qian et al. (2004) reported an anomalous relationship between hardness and wear properties of a superelastic NiTi alloy. This high wear-resistant property is also related to the reversible transformation in this material (Yan, 2006) and is believed to have many exciting applications in tribological engineering (Li, 2000).

With the growing application of superelastic NiTi SMA in small dimensions such as MEMS and surface engineering, micro-indentation and nano-indentation techniques play an important role in probing the mechanical properties of SMA. For example, Gall et al. (2001) studied the instrumented Vikers micro-indentation of single crystal NiTi SMA. Ni et al. (2003) reported their indentation experimental results of a NiTi alloy. The dynamic indentation response of NiTi films sputtered on oxidized silicon substrates was examined by Ma and Komvopoulos (2004). The superior wear-resistance of NiTi SMA and the background of its application in MEMS and surface engineering stimulated the present research to theoretically and numerically investigate the indentation behavior of superelastic NiTi. We choose a spherical indenter to avoid plastic deformation so as to concentrate on the relationship between the indentation response and the elastic and phase transformation properties of the material. In our investigation, dimensional analysis is first applied to establish the scaling relationships for spherical indentation. The finite element simulations are then carried out to obtain numerical results of the established scaling relationships.

2. Superelastic constitutive model

The superelastic behavior of an SMA can be illustrated by a stress–strain curve under a uniaxial loading–unloading cycle. A typical experimental superelastic curve from a tensile test is shown in Fig. 1(a). The tensile strain due to elastic deformation and transformation can recover completely after the removal of tensile stress for a superelastic SMA. In our theoretical and numerical study, an idealized mathematic model is used to describe this superelastic behavior as depicted in Fig. 1(b). Experimental studies have indicated that there exist a certain asymmetry between tension and compression for superelasticity. We do not distinguish this difference in this paper for simplicity, which implies that the material under uniaxial compression is assumed to obey the idealized model as well. Considering that the material under an indenter is mainly in compression, not partly in tension and partly in compression, such an assumption will not affect the results significantly. The martensite transformed from austenite under indentation force may experience reorientation during further loading. Since the strain due to reorientation is relatively small as compared with the forward transformation strain, we do not explicitly distinguish the reorientation strain from the total recoverable transformation strain in our model.

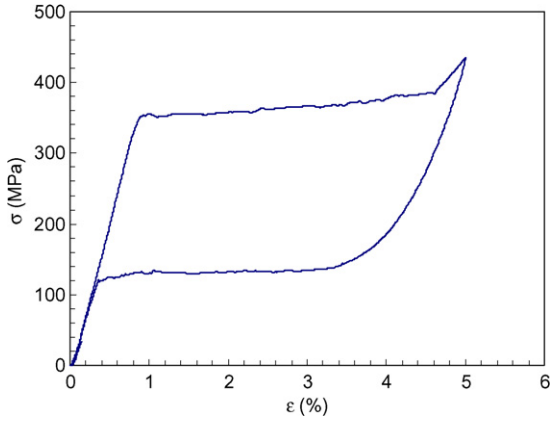

Fig. 1(a). A typical superelastic stress–strain curve from a uniaxial tensile test of NiTi SMA.

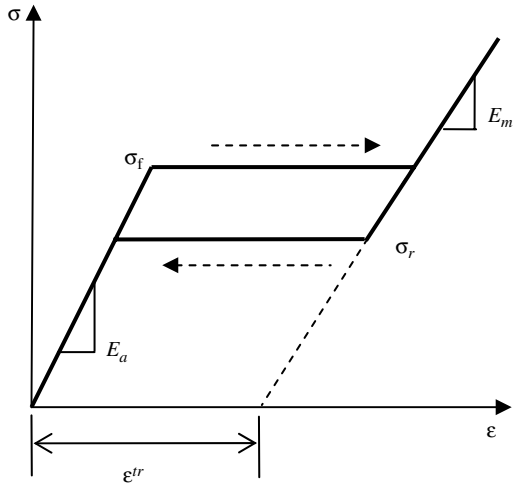

Fig. 1(b). Illustration of an idealized perfectly superelastic model under uniaxial tension and the definitions of the material parameters.

Referring to Fig. 1(b), the forward transformation and reverse transformation processes are simplified as perfect, that is, the forward transformation stress σ_f and the reverse transformation stress σ_r remain constant during the forward and reverse transformations, respectively. In our mathematic model, the material parameters to define the superelastic behavior of an SMA are listed below:

σ_f forward transformation stress from austenite to martensite
σ_r reverse transformation stress from martensite to austenite
ε^{tr} maximum transformation strain in uniaxial tension or maximum magnitude of the transformation strain tensor, i.e., $\varepsilon^{tr} = \left(\frac{2}{3}\varepsilon^{tr}_{ij}\varepsilon^{tr}_{ij}\right)^{0.5}$. In the case of uniaxial tension and neglecting transformation volume strain ($\varepsilon^{tr}_{ij} = 0$), we have $\varepsilon^{tr} = \varepsilon^{tr}_{11}$.
E_a elastic modulus of the austenite
E_m elastic modulus of the martensite
ν_a elastic Poisson's ratio of the austenite
ν_m elastic Poisson's ratio of the martensite

Except the Poisson's ratios, which reflect the coupling elastic deformation in the directions perpendicular to the loading direction, all these parameters are illustrated in the one-dimensional stress–strain curve in Fig. 1(b) and their values can be determined from an experimental tensile test. The transformation volume strain is

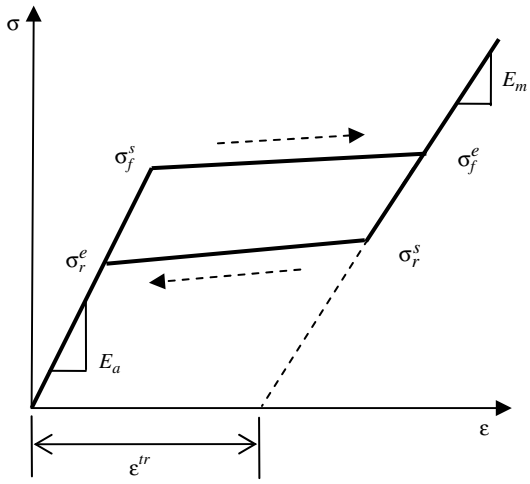

Fig. 1(c). Illustration of an idealized linear hardening superelastic model under uniaxial tension.

normally much smaller than the transformation shear strain components. For example, the transformation volume strain equals −0.37% for CuAlNi SMA according to the calculation of Fang et al. (1998). The volume strain for NiTi SMA is about −0.39% according to the measurement by Holtz et al. (1999). Therefore, the transformation volume strain is neglected in our analysis. Since this is a perfect transformation model, there is no hardening during the transformation process. Practically, a certain transformation hardening can be observed in some SMAs. If we consider transformation hardening, at least two more material properties should be introduced. In the simplest linear hardening case, we can introduce the starting and ending stresses, $\sigma_{\mathrm{f}}^{\mathrm{s}}$ and $\sigma_{\mathrm{f}}^{\mathrm{e}}$, for the forward transformation, and $\sigma_{\mathrm{r}}^{\mathrm{s}}$ and $\sigma_{\mathrm{r}}^{\mathrm{e}}$ for the reverse transformation, see Fig. 1(c). In our later numerical calculations, we use the perfect transformation model, but the main results from the theoretical analysis are also valid for transformation hardening materials as discussed in the next section.

The model in Fig. 1(b) or 1(c) is one-dimensional. In our theoretical study of spherical indentation on a superelastic alloy such as polycrystalline NiTi, a three-dimensional superelastic transformation model is required. Research on the constitutive model for transformation behavior in SMA has been conducted for decades. Numerous mathematical models can be found in literatures, such as, Liang and Rogers (1990), Brinson and Lammering (1993), Sun and Hwang (1993) and Yan et al. (1998). To avoid the complexity of tracking the detailed evolution of the material microstructure during phase transformations, a phenomenological model developed by Auricchio and Taylor (1997) and Auricchio et al. (1997) is adopted in the present investigation. This phenomenological model can describe the macroscopic superelastic and shape memory deformation behaviors of an SMA due to microstructural phase transformation or reorientation. It is well verified and implemented in the finite element package ABAQUS (2004). In our present indentation modeling and simulation, any size-dependent effects are assumed to be insignificant. It is worthwhile to mention that size-dependent effects such as the strain gradient effect might appear in a nano-indentation test. To simulate the size effect, more complicated models should be adopted.

3. Indentation test with a spherical indenter tip

In the present investigation of the indentation test, we consider a spherical indenter tip. The spherical indenter has also been popularly applied to study other materials, see Alcala et al. (1998) and Zarudi et al. (2003). The reason to choose a spherical indenter tip is to avoid plastic deformation under a low indentation force. We can then focus our investigation on the indentation curve due to pure superelastic deformation, and reveal the relationships between superelastic indentation curve and the transformation behaviors of a superelastic SMA. The coupling behavior between transformation deformation and plastic deformation is quite complicated and is out of the scope of this paper. Some experimental observations and simple theoretical

modeling can be found respectively in McKelvey and Ritchie (2001) and Yan et al. (2003). Spherical indenter tips are commercially available. A typical superelastic indentation curve by a spherical indenter from our experimental test is shown in Fig. 2. In this indentation test, the maximum indentation force is just over 10 000 μN and the corresponding indentation depth is about 120 nm. As we can see, the indentation curve demonstrates superelasticity with a hysteresis loop similar to that in a uniaxial tension. This means that the material transformed to martensite in the loading process can transform completely back to its original austenite state.

The indenter tip is normally made of diamond. Since the Young's modulus of a diamond is much larger than that of SMAs, we assume that the diamond is rigid in our theoretical analysis. Generally, the elasticity of the diamond can still be considered by introducing an equivalent Young's modulus for the specimen which combines the real Young's moduli of the specimen and the indenter while still assuming the indenter is rigid, see Johnson (1985). An enlarged view of indentation into a superelastic SMA is illustrated in Fig. 3. As the indentation depth and the size of the indentation area are much smaller than the size of the SMA specimen, the specimen is treated as a semi-infinite body. Due to the deformation of the material, the indenter displacement, that is, the indentation depth h, is different from the local vertical surface displacement of the specimen, h_c, along which contact is made. If h is smaller than h_c, then "pile-up" of the surface profiles occurs, as illustrated in Fig. 3. On the contrary, if h is larger than h_c, then this phenomenon is called "sink-in". The degree of "sink-in" or "pile-up" depends on the plastic yield stress and the level of the strain-hardening for ordinary elastic–plastic materials, see Giannakopoulos and Suresh (1999). Recent indentation tests by Huang et al.

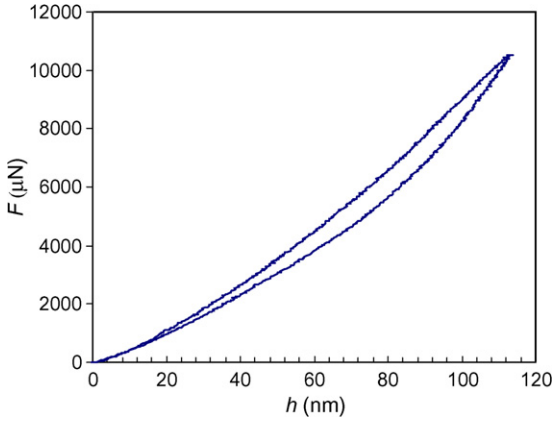

Fig. 2. A typical experimental superelastic indentation curve from a micro-indentation test of a superelastic NiTi with tip radius $R = 50$ μm.

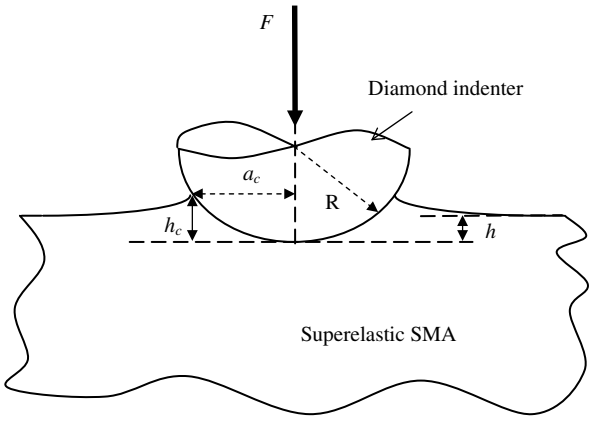

Fig. 3. Illustration of a spherical indentation test of a superelastic SMA.

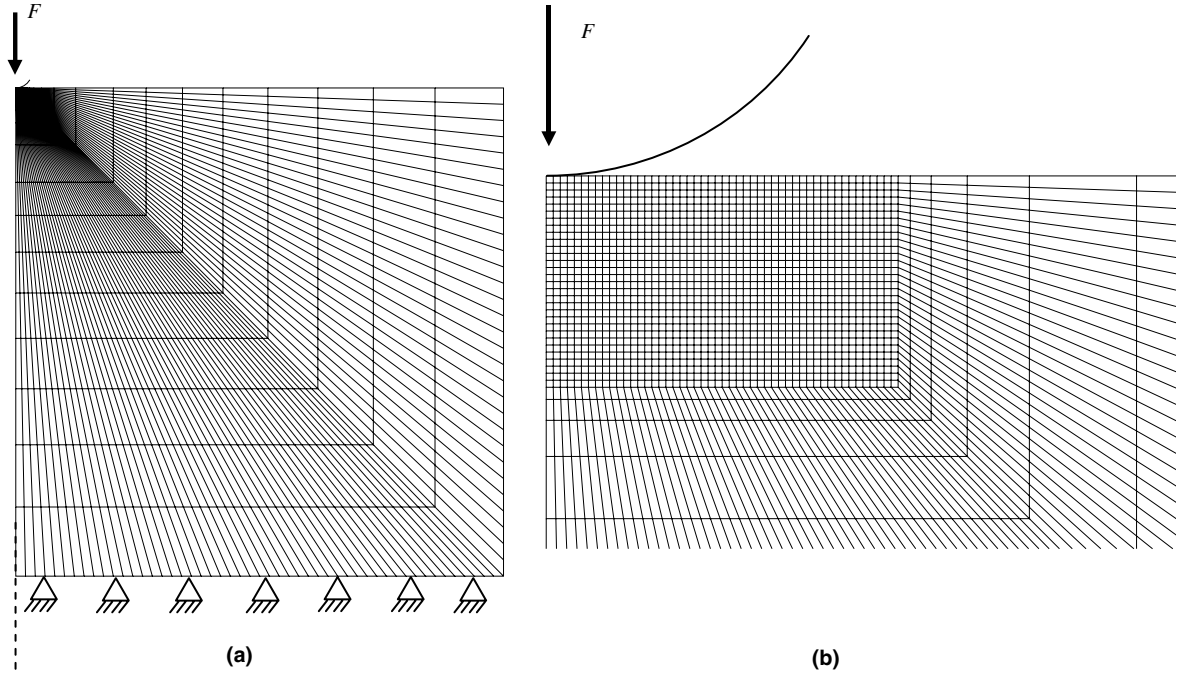

Fig. 4. Axisymmetric finite element model to simulate the indentation test with a rigid spherical indenter: (a) the entire finite element mesh and boundary conditions; (b) the fine mesh near the intender tip.

(2005) found that "pile-up" appears at a high temperature and "sink-in" appears at a low temperature in NiTi due to the influence of temperature on the transition. Here, we only consider that the indentations are carried out at a given temperature. The variable a_c in Fig. 3 represents the radius of the contact area.

A recent study by Bucaille et al. (2003) found that friction has no significant influence on the indentation for elastic–plastic materials if the included angle is equal to or higher than 60°. Here we are considering a spherical indenter with an included angle of 90°. Therefore, a frictionless assumption is made between the indenter and the specimen in our simulations. The finite element numerical method is utilized to simulate the indentation. In our numerical study, the axisymmetric condition is applied. Fig. 4 illustrates the finite element model. The size of the entire model is much larger than the radius of the indentation tip and the size of the transformation zone. The bottom of the model is therefore constrained in both the radial and axial directions. As demonstrated in Fig. 4b, a very fine mesh with the shortest element side of 0.1 μm is employed in the transformation zone beneath the indenter tip to ensure the accuracy of the numerical results. The model contains a total of 2940 four-noded axisymmetric elements. Testing results for elastic contact are verified by comparison with the Hertz contact theory.

4. Indentation analysis and numerical results

Dimensional analysis has been successfully applied to study the indentation on ordinary materials. For conical indenters, the established scaling relationships from dimensional analysis show that the indentation force is proportional to the square of the indenter displacement and that the hardness under load is independent of indenter displacement (Cheng and Cheng, 1998). Tunvisut et al. (2001) utilized dimensional analysis and the finite element method to determine the mechanical properties of thin coatings from microindentation tests. Dimensional analysis was also applied by Dao et al. (2001) to establish forward and reverse analysis algorithms for studying instrumented sharp indentation. In the following subsections, we will show that dimensional analysis is still a powerful tool for the spherical indentation of superelastic SMA.

4.1. Indentation curve

Generally, the indentation force F during loading process depends on the superelastic properties of the material quantified by the parameters σ_f, σ_r, E_a, E_m, ε^{tr}, ν_a, ν_m as well as the indentation depth h and the indenter radius R, i.e.,

$$F = Z(\sigma_f, \sigma_r, E_a, E_m, \nu_a, \nu_m, \varepsilon^{tr}, h, R). \tag{1a}$$

During the initial stage of indentation and before the start of forward transformation, the material is in an elastic state. In the elastic contact regime, we generally have

$$F = Z^e(E_a, \nu_a, h, R). \tag{1b}$$

Within the limits of small deformation, the Hertz contact theory can be applied to describe this purely elastic contact problem. Referring to Johnson (1985), the elastic indentation force is therefore determined by

$$F = \frac{4}{3} E_a^* R^{1/2} h^{3/2}, \tag{2}$$

where $E_a^* = \frac{E_a}{1-\nu_a^2}$. As we expect, the transformation properties of the material, including the transformation stresses σ_f and σ_r, the maximum magnitude of the transformation strain ε^{tr} in this stage and the elastic constants of the martensite E_m and ν_m, make no contribution to the elastic indentation force. For a sharp indenter, such as conical and pyramidal indenters, the indentation force is proportional to the square of the indentation depth, $F \propto h^2$. Due to the introduction of another geometrical dimension, the radius of the spherical indenter tip, this conclusion does not hold any more for a spherical indenter.

With the increase of the indentation depth or the indentation force, the magnitude of the stress increases in the specimen. Once the equivalent stress at a point inside the specimen reaches the forward transformation stress, the material at that point will start to transform to martensite (Auricchio and Taylor, 1997). The martensite volume fraction will increase at that point until it reaches unity. Meanwhile, the martensite zone will extend. During the entire loading process, that is, the monotonic increase in the indentation depth with loading, we can reasonably assume that the magnitude of strains at any material point in the specimen will increase monotonically and gradually. The reverse transformation and elastic unloading will not occur anywhere in the specimen during a loading process, that is, the reverse transformation makes no contribution to the indentation loading force. Therefore, the functional relationship to determine the indentation loading force in this stage can be simplified as,

$$F = Z'(\sigma_f, E_a, E_m, \varepsilon^{tr}, \nu_a, \nu_m, h, R). \tag{3}$$

According to Buckingham Π theorem for dimensional analysis, we choose E_a and R as the primary quantities in our problem with two fundamental dimensions, length and force. The dimensionless scaling relationship for the indentation loading force is

$$\frac{F}{R^2 E_a} = \Pi_1\left(\frac{\sigma_f}{E_a}, \frac{E_m}{E_a}, \varepsilon^{tr}, \nu_a, \nu_m, \frac{h}{R}\right). \tag{4a}$$

At the end of the loading process, when the indentation depth reaches the maximum value h_m, the corresponding maximum indentation force F_m can be expressed as

$$\frac{F_m}{R^2 E_a} = \Pi_2\left(\frac{\sigma_f}{E_a}, \frac{E_m}{E_a}, \varepsilon^{tr}, \nu_a, \nu_m, \frac{h_m}{R}\right). \tag{4b}$$

Finite element simulations were carried out to study the derived dimensionless function (4b). In all of the following numerical simulations, the values of ν_a and ν_m were fixed at 0.3, which is reasonable for SMAs, and the default value for h_m/R is 0.02. Some of the numerical results of the above dimensionless function are shown in Fig. 5. Fig. 5(a) indicates that the normalized maximum indentation force $F_m/(R^2E_a)$ decreases with the increase in the maximum magnitude of the transformation strain ε^{tr}, especially when ε^{tr} is less than 5%. The influence of ε^{tr} on $F_m/(R^2E_a)$ vanishes if ε^{tr} reaches about 6%. This is due to the fact that the transformation strain in the part of the transformed material can no longer increase under the given indentation depth

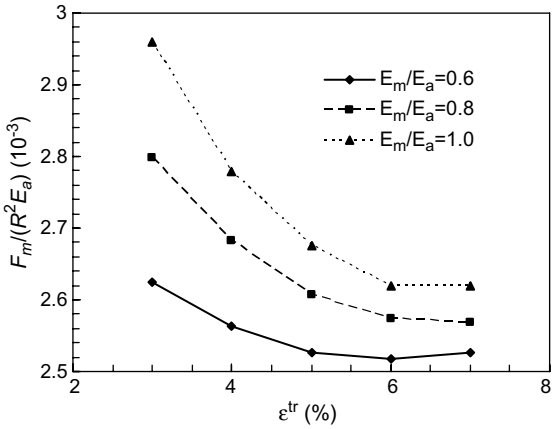

Fig. 5(a). Relationship between the normalized maximum indentation force $F_m/(R^2E_a)$ and the maximum magnitude of the transformation strain ε^{tr}. In all the cases, $\sigma_f/E_a = 0.012$.

$h_m = 0.02R$. It is expected that the influencing range of ε^{tr} on $F_m/(R^2E_a)$ will be extended if we increase the indentation depth, h_m/R. Fig. 5(a) also indicates that the maximum indentation force $F_m/(R^2E_a)$ increases with the Young's modulus of the martensite E_m/E_a for the given value of ε^{tr}. Fig. 5(b) shows the relationship between normalized maximum indentation force $F_m/(R^2E_a)$ and the normalized forward transformation stress σ_f/E_a for $\varepsilon^{tr} = 4\%$. As we expect, the maximum indentation force increases with the forward transformation stress.

During the unloading stage, the material starts to transform back from martensite to austenite once the stress reaches the reverse transformation stress σ_r. Therefore, the reverse transformation stress σ_r now affects the indentation unloading response F. Additionally, the unloading begins after the indenter reaches the maximum displacement h_m. The indentation unloading force is also a function of the maximum indentation depth. The dimensionless function for the indentation unloading force can be derived as

$$\frac{F}{R^2E_a} = \Pi_3\left(\frac{\sigma_f}{E_a}, \frac{\sigma_r}{E_a}, \frac{E_m}{E_a}, \varepsilon^{tr}, \nu_a, \nu_m, \frac{h_m}{R}, \frac{h}{R}\right). \tag{5}$$

The initial unloading slope is of extraordinary interest for ordinary materials. It is simply related to the Young's modulus and the contact area in indentations of elastic–plastic materials, see Oliver and Pharr

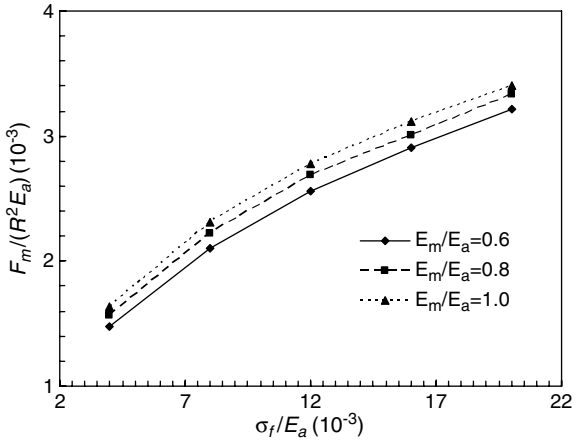

Fig. 5(b). Relationship between the normalized maximum indentation force $F_m/(R^2E_a)$ and the normalized forward transformation stress σ_f/E_a. In all the cases, $\varepsilon^{tr} = 4\%$.

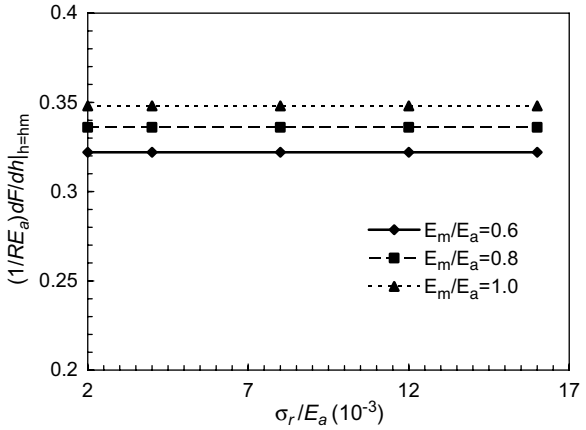

Fig. 6(a). Relationship between the normalized initial unloading slope $\frac{1}{RE_a}\frac{dF}{dh}\big|_{h=hm}$ and the normalized reverse transformation stress σ_r/E_a. In all the cases, $\varepsilon^{tr} = 4\%$ and $\sigma_f/E_a = 0.02$.

(1992) and Cheng and Cheng (1997). In the current superelastic indentation, the dimensionless function for the unloading slope at the onset of unloading is

$$\left.\frac{1}{RE_a}\frac{dF}{dh}\right|_{h=h_m} = \Pi_4\left(\frac{\sigma_f}{E_a}, \frac{\sigma_r}{E_a}, \frac{E_m}{E_a}, \varepsilon^{tr}, \nu_a, \nu_m, \frac{h_m}{R}\right). \tag{6a}$$

Our numerical results indicate that the reverse transformation stress σ_r does not affect the initial unloading slope. As shown in Fig. 6(a), the normalized unloading slope does not change with different values of the normalized reverse transformation stress in all three cases with different values of E_m/E_a. This conclusion is due to the fact that physically the reverse transformation process has not yet started at the onset of unloading because of the hysteresis as shown in Fig. 1 (except $\sigma_r = \sigma_f$). Therefore, Eq. (6a) can be further simplified as

$$\left.\frac{1}{RE_a}\frac{dF}{dh}\right|_{h=h_m} = \Pi_4'\left(\frac{\sigma_f}{E_a}, \frac{E_m}{E_a}, \varepsilon^{tr}, \nu_a, \nu_m, \frac{h_m}{R}\right). \tag{6b}$$

The relationship between the normalized initial unloading slope $\frac{1}{RE_a}\frac{dF}{dh}\big|_{h=hm}$ and the maximum magnitude of the transformation strain tensor ε^{tr} for a indicates given $\sigma_f/E_a = 0.012$ is shown in Fig. 6(b). It indicates that $\frac{1}{RE_a}\frac{dF}{dh}\big|_{h=hm}$ is insensitive to ε^{tr}. Fig. 6(c) shows the influence of the normalized forward transformation stress

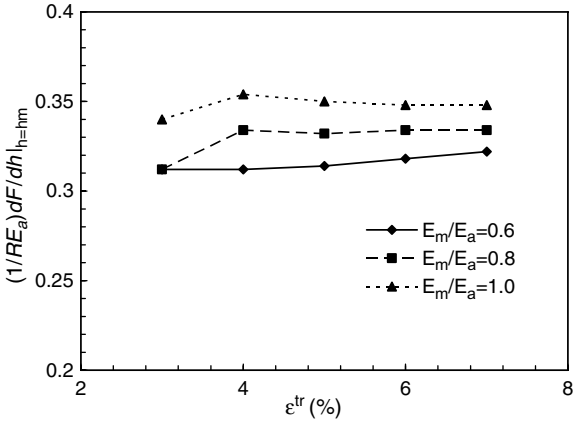

Fig. 6(b). Relationship between the normalized initial unloading slope $\frac{1}{RE_a}\frac{dF}{dh}\big|_{h=hm}$ and the maximum magnitude of the transformation strain ε^{tr}. In all the cases, $\sigma_f/E_a = 0.012$.

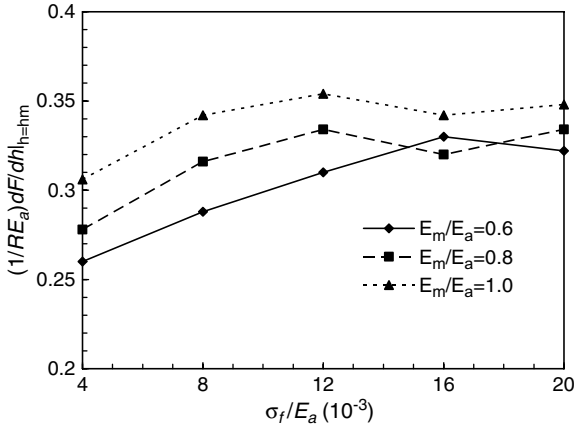

Fig. 6(c). Relationship between the normalized initial unloading slope $\frac{1}{RE_a}\frac{dF}{dh}\big|_{h=hm}$ and the normalized forward transformation stress σ_f/E_a. In all the cases, $\varepsilon^{tr} = 4\%$.

σ_f/E_a on the normalized initial unloading slope $\frac{1}{RE_a}\frac{dF}{dh}\big|_{h=hm}$. In all the cases in Fig. 6(c), $\varepsilon^{tr} = 4\%$. As we can see, the initial unloading slope increases with the forward transformation stress until σ_f/E_a reaches 0.016. All the numerical results in Figs. 6(a)–6(c) indicate that the normalized unloading slope increases with the normalized martensite's Young's modulus except one case in Fig. 6(c). This exception might be caused by numerical error.

4.2. Bifurcation force and return force

4.2.1. Bifurcation force and its determination

The pure elastic loading curve at the beginning of the loading process is determined by Eq. (2). Once the material in the specimen starts to transform to martensite, the indentation loading curve will begin to deviate from the elastic loading curve as demonstrated in Fig. 7(a), where both the elastic indentation curve and superelastic indentation curve with the same indenter tip are depicted. The elastic curve is obtained from Eq. (2) and the superelastic curve is from a finite element simulation with the same elastic properties for the austenite. A bifurcating point can be defined as the point at which the superelastic indentation loading curve starts to deviate from the elastic indentation curve, see Fig. 7(b). The force corresponding to the bifurcating point is called bifurcation force F_b, as illustrated in Fig. 7(b). The bifurcation point corresponds to the onset of plasticity for ordinary elastic–plastic materials. Some experimental investigations on the onset of plasticity under nanoindentation were carried out recently, e.g., Carcia-Manyes et al. (2005).

Because this bifurcating point signals the start of forward transformation in the material, it is an important characteristic point in a superelastic indentation curve. The bifurcation force, F_b, should not rely on the properties of the product phase, that is, the elastic Young's modulus and Poisson ratio of martenite. Furthermore, it does not depend on the hardening behavior shown in Fig. 1(c) of the forward transformation process, nor the maximum magnitude of the transformation strain ε^{tr}. In a certain sense, the quantity F_b is similar to the initial transformation stress σ_f in Fig. 1. However, the bifurcation force is the response of the indenting structure, which should also rely on the property of the austenite and the geometry of the indenter. Generally, we have the following relationship:

$$F_b = Y(\sigma_f, E_a, \nu_a, h_b, R). \tag{7}$$

The corresponding dimensionless function is

$$\frac{F_b}{R^2 E_a} = \Pi_5\left(\frac{\sigma_f}{E_a}, \frac{h_b}{R}, \nu_a\right). \tag{8}$$

Considering the fact that the bifurcating point is also on the elastic indentation curve, the bifurcation force F_b should also satisfy the following elastic indentation scaling function

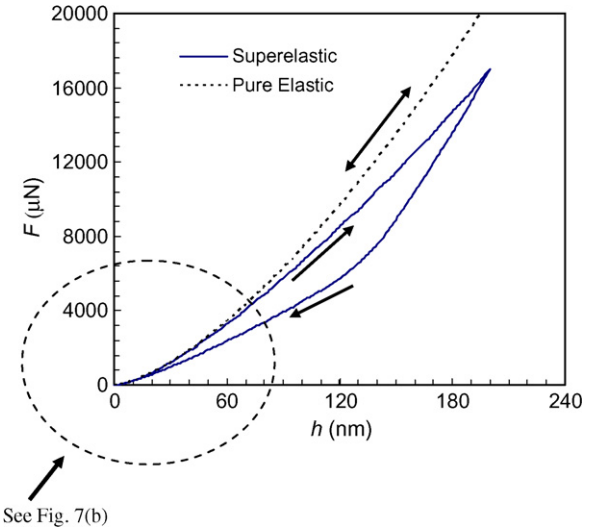

Fig. 7(a). Comparison between a pure elastic indentation curve and a superelastic indentation curve with the same elastic constants for the austenite.

$$\frac{F_b}{R^2 E_a} = \Pi_5^e\left(\frac{h_b}{R}, \nu_a\right), \tag{9}$$

which can be derived from Eq. (1b). From Eqs. (8) and (9), we can establish a scaling relationship so that the dimensionless variable $F_b/(R^2E_a)$ only relies on σ_f/E_a and ν_a as

$$\frac{F_b}{R^2 E_a} = \Pi_5'\left(\frac{\sigma_f}{E_a}, \nu_a\right). \tag{10a}$$

It is worth mentioning that the bifurcation force does not depend on the indentation depth according to Eq. (10a). Generally, the dimensionless function Eq. (10a) can be easily determined numerically from finite element simulations. Within the limits of small deformation, the above relationship can be analytically obtained by applying Hertz contact theory. According to Johnson (1985), we have

$$\frac{F_b}{R^2 E_a} = 17.92\left(\frac{\sigma_f}{E_a}\right)^3 \tag{10b}$$

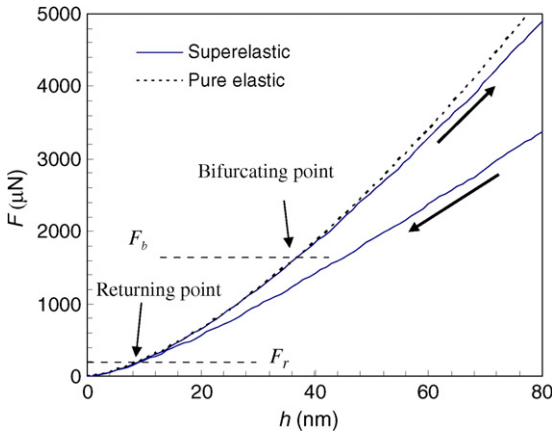

Fig. 7(b). Definition of the bifurcation force F_b and the return force F_r.

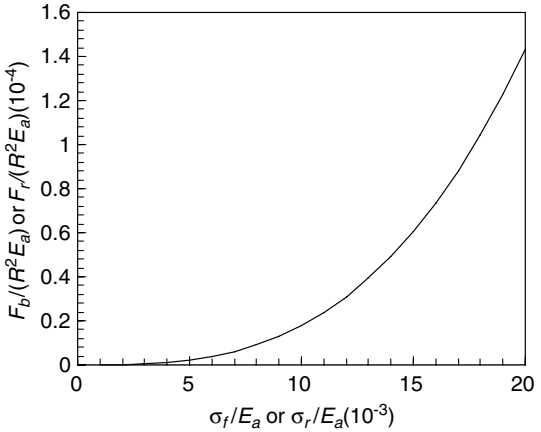

Fig. 8. Relationship between the normalized bifurcation force $F_b/(R^2E_a)$ and the normalized forward transformation stress σ_f/E_a for $\nu_a = 0.3$ within small deformation. (This curve also represents the relationship between the normalized return force $F_r/(R^2E_a)$ and the normalized reverse transformation stress σ_r/E_a if we simply change the x-axis title to σ_r/E_a and the y-axis title to $F_r/(R^2E_a)$.)

for $\nu_a = 0.3$ as shown in Fig. 8. Obviously, the value of $F_b/(R^2E_a)$ increases with σ_f/E_a, which means that a higher forward transformation stress will result in a higher bifurcation force, or vice versa. This simple relationship can be used to calibrate the forward transformation stress of the superelastic SMA from a measured superelastic indentation curve. It should be noted that practically it would be difficult to detect the bifurcating point from an indentation curve. This problem could be solved by checking the indentation slope curve. A detailed procedure on how to calibrate superelastic material properties from spherical indentation tests is discussed elsewhere (Yan et al., 2006).

4.2.2. Return force and its determination

During the unloading process, the martensite phase will become unstable and transform back to the original austenite phase before the load reduces to zero. After the completion of the reverse transformation, the unloading curve will eventually return to the pure elastic loading–unloading curve, as shown in Fig. 7. The returning point, defined as the first point where the unloading curve re-enters the elastic curve, indicates the completion of the reverse transformation process in the material. The indentation force corresponding to the returning point is named as the return force F_r, see Fig. 7(b). The return force F_r is another important quantity in a superelastic indentation curve. In Appendix A, we prove that the return force F_r does not depend on σ_f, E_m, ν_a, ε^{tr} and transformation hardening behaviors. In other words, the return force does not depend on the transformation history. It only relies on the reverse transformation stress, σ_r, and the elastic constants of the austenite, E_a and ν_a. Mathematically, we have

$$\frac{F_r}{R^2E_a} = \Pi_6\left(\frac{\sigma_r}{E_a}, \nu_a\right). \tag{11}$$

To sum up the above analyses, we have two important conclusions:

(1) The bifurcation force, F_b, only depends on the forward transformation stress σ_f, the elastic constants of the austenite E_a and ν_a and the radius of the indenter R. The functional relationship is given by Eq. (10) and it is shown in Fig. 8 in the case of $\nu_a = 0.3$ with small deformation.
(2) The return force F_r only depends on the reverse transformation stress σ_r, the elastic constants of the austenite E_a and ν_a and the radius of the indenter R, given by Eq. (11).

Now, let us consider two superelastic materials with the same elastic constants E_a and ν_a for the austenite, but different transformation stresses. The forward transformation stress of material (2) is equal to the reverse transformation stress of material (1),

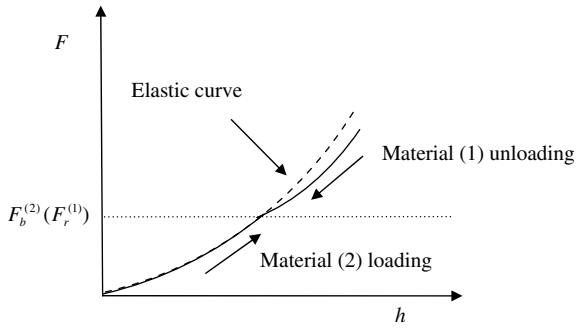

Fig. 9. Schematics of the coincidence of the returning point of material one with the bifurcating point of material two.

$$\sigma_{\mathrm{f}}^{(2)} = \sigma_{\mathrm{r}}^{(1)} = \sigma. \tag{12}$$

Because both materials have the same austenite, the elastic parts of their indention curves should be identical for both materials. Following the loading curve of the second material starting from the elastic stage, as illustrated in Fig. 9, once the maximum equivalent stress the in material reaches the forward transformation stress $\sigma_{\mathrm{f}}^{(2)}$, the indentation curve starts to deviate from the elastic curve. At this critical bifurcating point the stress field in the material is still an elastic one. The corresponding bifurcation force is $F_{\mathrm{b}}^{(2)}$. On the other hand, we follow the unloading curve of material (1). At the returning point, upon the completing of the reverse transformation, the stress field in material (1) can also be treated as an elastic one with the maximum equivalent stress equal to $\sigma_{\mathrm{r}}^{(1)}$. Referring to Eq. (12), both elastic fields have the same magnitude of a maximum equivalent stress. According to the uniqueness theorem of the solution for an elastic stable problem (Sokolnikoff, 1983), the elastic field in material (1) can also be considered as the one obtained by applying the loading force from zero to $F_{\mathrm{r}}^{(1)}$. In the current elastic contact problem, the magnitude of the external indentation loading force that leads to a given maximum equivalent stress in the material can be uniquely determined. Therefore, we have

$$F_{\mathrm{b}}^{(2)} = F_{\mathrm{r}}^{(1)}. \tag{13}$$

According to Eqs. (10a), (11) and (13), we obtain the following relationship

$$\Pi_5'\left(\frac{\sigma}{E_{\mathrm{a}}}, \nu_{\mathrm{a}}\right) = \Pi_6\left(\frac{\sigma}{E_{\mathrm{a}}}, \nu_{\mathrm{a}}\right). \tag{14}$$

Since the value of σ in the above equation is arbitrary, it can be concluded that the dimensionless function Π_5' to determine the bifurcation force is identical to the dimensionless function Π_6 to determine the return force. Within the limits of small deformation, similar to Eq. (10b), we have the following analytical solution

$$\frac{F_{\mathrm{r}}}{R^2 E_{\mathrm{a}}} = 17.92\left(\frac{\sigma_{\mathrm{r}}}{E_{\mathrm{a}}}\right)^3 \tag{15}$$

for $\nu_{\mathrm{a}} = 0.3$ as shown in Fig. 8.

Generally, the simple relationship of Eq. (11) can be applied to calibrate the reverse transformation stress from a measured indentation unloading curve after the return force is determined. This is discussed in detail elsewhere (Yan et al., 2006).

4.3. Hardness analysis

To measure the hardness of materials has long been a major purpose of indentation tests with different indenter tips (Tabor, 1996). The hardness H is normally defined as the mean pressure the material will support under a load (Oliver and Pharr, 1992),

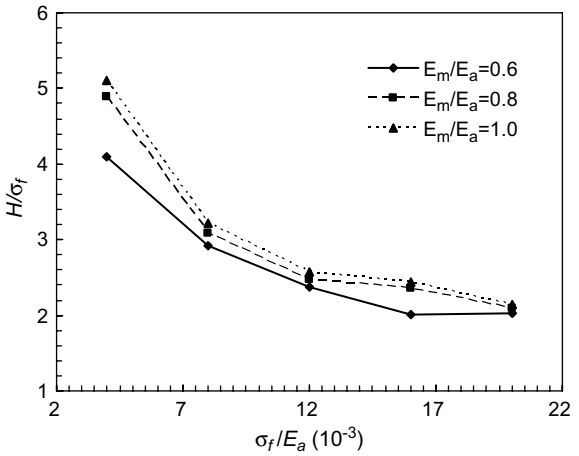

Fig. 10. Relationship between the ratio of the hardness to the forward transformation stress H/σ_f and the normalized forward transformation stress σ_f/E_a with fixed ε^{tr} of 4%.

$$H = \frac{F_m}{A_c}, \tag{16}$$

where F_m is the maximum indentation force, which can be determined by Eq. (4b). A_c is the projected area of contact under the maximum indentation force F_m. As illustrated in Fig. 3, A_c is equal to πa_c^2 for the current spherical indenter.

Based on its definition of Eq. (16), similar to the previous analysis for the peak indentation force F_m, the hardness H does not depend on the reverse transformation process, that is, it has nothing to do with reverse transformation stress σ_r. The dimensionless function to determine the hardness H is expressed as

$$\frac{H}{E_a} = \Pi_8\left(\frac{\sigma_f}{E_a}, \frac{E_m}{E_a}, \varepsilon^{tr}, \nu_a, \nu_m, \frac{h_m}{R}\right). \tag{17}$$

Previous research reveals that the hardness measured from a conical indenter is independent of the maximum indentation depth h_m, see Cheng and Cheng (1999). The above relationship clearly indicates that such a conclusion is not suitable for a spherical indenter. That is, the hardness measured from a spherical indenter will depend on the indentation depth.

The ratio of hardness to the plastic yield strength is an interesting variable for ordinary metals and it is around 3.0, see Tabor (1996) and Johnson (1985). Here for superelastic materials, the functional relationship of the ratio H/σ_f can be expressed as

$$\frac{H}{\sigma_f} = \frac{E_a}{\sigma_f}\Pi_8\left(\frac{\sigma_f}{E_a}, \frac{E_m}{E_a}, \varepsilon^{tr}, \nu_a, \nu_m, \frac{h_m}{R}\right). \tag{18}$$

The numerical results for this ratio versus σ_f/E_a are shown in Fig. 10, where $\varepsilon^{tr} = 4\%$ and $h_m/R = 0.02$. Fig. 10 reveals that the ratio H/σ_f decreases with the increase of the normalized forward transformation stress σ_f/E_a. In the reasonable range of $0.004 \leqslant \sigma_f/E_a \leqslant 0.016$, H/σ_f varies from about 5.1 to 2.1. Therefore, unlike the case of plasticity, the spherical hardness due to phase transformation cannot be used as a material constant to give a measure of the forward transformation stress. Fig. 10 also indicates that the Young's modulus of martensite can also affect the ratio slightly.

5. Conclusions

Dimensional analysis and the finite element approach are employed to study the spherical indentation of superelastic SMA. Several universal scaling functions to describe a superelastic indentation curve are established. Our results revealed several important relationships between indentation responses and material properties. The major conclusions from the present investigation are as follows:

(1) The maximum indentation force does not rely on the reverse transformation stress.
(2) The initial unloading slope does not rely on the reverse transformation stress.
(3) The bifurcation force, which indicates the start of forward transformation in a superelastic indentation curve, only depends on the forward transformation stress, the elastic properties of the austenite and the indenter geometry.
(4) The return force, which indicates the finish of the reverse transformation in a superelastic indentation curve, only relies on the reverse transformation stress, the elastic properties of the austenite and the indenter geometry.
(5) The dimensionless scaling function to determine the bifurcation force is identical to the dimensionless scaling function to determine the return force.
(6) Generally, the universal scaling function for the bifurcation force and the return force can be numerically determined. In the case of small deformation, this function can be determined analytically from elastic solutions.

Acknowledgements

The numerical calculations were carried out at the National Facility of the Australian Partnership for Advanced Computing through an award under the Merit Allocation Scheme to WY. This work was financially supported by the Research Grants Council of Hong Kong (Project Nos.: HKU6199/03E and 619705), the National Natural Science Foundation of China (Grant Nos.: 50305029 and 11021202) and the Education Ministry of China. The authors are grateful to the two unknown reviewers for their helpful comments for improving the manuscript.

Appendix A

Without plastic deformation and within the frame of small deformation, the total strain inside an indented superelastic SMA generally consists of two parts, the elastic strain and the transformation strain, i.e.,

$$\varepsilon_{ij} = \varepsilon^{\mathrm{e}}_{ij} + \varepsilon^{\mathrm{tr}}_{ij}. \tag{A.1}$$

The stress field can be determined by the elastic strain through Hooke's law, i.e.,

$$\sigma_{ij} = E_{ijkl}\varepsilon^{\mathrm{e}}_{kl}, \tag{A.2}$$

where E_{ijkl} is the elastic stiffness tensor.

Now, consider the unloading indentation curve. When the returning point is indefinitely approached during unloading, see Fig. 7(b), the transformation strain at any material point should be zero or infinitely approaching zero in our current problem without any singular points, i.e., $\varepsilon^{\mathrm{tr}}_{ij} \to 0$, or $\varepsilon_{ij} \approx \varepsilon^{\mathrm{e}}_{ij}$. That is, the deformation field at this moment can be treated as an elastic deformation field. Based on the reverse transformation condition, the maximum equivalent stress in the field should be equal to the reverse transformation stress σ_{r}. For a reverse transformation hardening material, this value will be the reverse transformation ending stress $\sigma^{\mathrm{e}}_{\mathrm{r}}$, see Fig. 1(c). Therefore, at the returning point, we have an elastic field with the maximum equivalent stress equaling to σ_{r}.

On the other hand, let us consider an elastic loading problem. We increase the indentation force elastically from zero to F_{r}. According to the uniqueness theorem of the solution for an elastic stable problem with the same geometry, elastic properties of material and boundary conditions, the solution to the elastic problem is unique for a given load. In the current case, it indicates that the solution to the elastic field from the elastic loading to the returning point should be the same as the one we obtained from reverse transformation unloading to the returning point. Following the elastic loading path, we can conclude that the value of the return force F_{r}, which corresponds to an elastic field with the maximum equivalent stress of σ_{r}, does not depend on the forward and reverse transformation history, i.e., F_{r} does not depend on the maximum indentation depth h_{m}, the forward transformation stress σ_{f}, the maximum magnitude of the transformation strain, the Young's modulus of the martensite E_{m}, and its Poisson's ratio ν_{m}. It only

depends on the indenter radius R, the elastic constants of the austenite E_a and v_a, and the reverse transformation stress σ_r, or the reverse transformation ending stress for a reverse σ_r^e transformation hardening material. Mathematically, we have

$$\frac{F_r}{R^2 E_a} = \Pi_6\left(\frac{\sigma_r}{E_a}, v_a\right). \tag{A.3}$$

References

ABAQUS version 6.4, 2004, Hibbitt, Karlsson and Sorensen, Providence, RI.

Alcala, J., Giannakopoulos, A.E., Suresh, S., 1998. Continuous measurements of load–penetration curves with spherical microindenters and the estimation of mechanical properties. Journal of Materials Research 13, 1390–1400.

Auricchio, F., Taylor, R.L., 1997. Shape-memory alloys: modelling and numerical simulations of the finite-strain superelastic behavior. Computer Methods in Applied Mechanics and Engineering 143, 175–194.

Auricchio, F., Taylor, R.L., Lubliner, J., 1997. Shape-memory alloys: macromodelling and numerical simulations of the superelastic behavior. Computer Methods in Applied Mechanics and Engineering 146, 281–302.

Brinson, L.C., Lammering, R., 1993. Finite-element analysis of the behavior of shape-memory alloys and their applications. International Journal of Solids and Structures 23, 3261–3280.

Bucaille, J.L., Stauss, S., Felder, E., Michler, J., 2003. Determination of plastic properties of metals by instrumented indentation using different sharp indenters. Acta Materialia 51, 1663–1678.

Carcia-Manyes, S., Guell, A.G., Gorostiza, P., Sanz, F., 2005. Nanomechanics of silicon surfaces with atomic force microscopy: an insight to the first stages of plastic deformation. Journal of the Chemical Physics 123, 114711.

Cheng, C.-M., Cheng, Y.T., 1997. On the initial unloading slope in indentation of elastic–plastic solids by an indenter with an axisymmetric smooth profile. Applied Physics Letters 71, 2623–2625.

Cheng, Y.-T., Cheng, C.-M., 1998. Effects of 'sinking in' and 'piling up' on estimating the contact area under load in indentation. Philosophical Magazine Letters 78, 115–120.

Cheng, Y.-T., Cheng, C.-M., 1999. Scaling relationships in conical indentation of elastic–perfectly plastic solids. International Journal of Solids and Structures 36, 1231–1243.

Dao, M., Chollacoop, N., Van Vliet, K.J., Venkatesh, T.A., Suresh, S., 2001. Computational modeling of the forward and reverse problems in instrumented sharp indentation. Acta Materialia 49, 3899–3918.

Fang, D.-N., Lu, W., Yan, W., Inoue, T., Hwang, K.-C., 1998. Stress–strain relation of CuAlNi SMA single crystal under biaxial loading—constitutive model and experiments. Acta Materialia 47, 269–280.

Fu, Y., Du, H., Huang, W., Zhang, S., Hu, M., 2004. TiNi-based thin films in MEMS applications: a review. Sensors and Actuators A 112, 395–408.

Gall, K., Juntunen, K., Maier, H.J., Sehitoglu, H., Chumlyakov, Y.I., 2001. Instrumented micro-indentation of NiTi shape-memory alloys. Acta Materialia 49, 3205–3217.

Giannakopoulos, A.E., Suresh, S., 1999. Determination of elastoplastic properties by instrumented sharp indentation. Scripta Materialia 40, 1191–1198.

Holtz, R.L., Sadananda, K., Imam, M.A., 1999. Fatigue thresholds of Ni–Ti alloy near the shape memory transition temperature. International Journal of Fatigue 21, s137–s145.

Huang, W.M., Su, J.F., Hong, M.H., Yang, B., 2005. Pile-up and sink-in in micro-indentation of a NiTi shape-memory alloy. Scripta Materialia 53, 1055–1057.

Jin, J., Wang, H., 1988. Wear resistance of Ni–Ti alloy. Acta Metallurgica Sinica 1, 76–81.

Johnson, K.L., 1985. Contact Mechanics. Cambridge University Press, London.

Li, D.Y., 2000. Exploration of TiNi shape memory alloy for potential application in a new area: tribological engineering. Smart Materials and Structures 9, 717–726.

Liang, C., Rogers, C.A., 1990. One-dimensional thermomechanical constitutive relations for shape memory materials. Journal of Intelligent Material Systems and Structures 1, 207–234.

Ma, X.-G., Komvopoulos, K., 2004. Pseudoelasticity of shape-memory titanium–nickel films subjected to dynamic nanoindentation. Applied Physics Letters 84, 4274–4276.

McKelvey, A.L., Ritchie, R.O., 2001. Fatigue-crack growth behavior in the superelastic and shape-memory alloy Nitinol. Metallurgical and Materials Transactions A 32, 731–743.

Ni, W., Cheng, Y.-T., Grummon, D.S., 2003. Microscopic superelastic behavior of a nickel–titanium alloy under complex loading conditions. Applied Physics Letters 82, 2811–2813.

Oliver, W.C., Pharr, G.M., 1992. An improved technique for determining hardness and elastic modulus using load and displacement sensing indentation experiments. Journal of Materials Research 7, 1564–1583.

Qian, L., Xiao, X., Sun, Q., Yu, T., 2004. Anomalous relationship between hardness and wear properties of a superelastic nickel–titanium alloy. Applied Physics Letters 84, 1076–1078.

Richman, R.H., Rao, A.S., Kung, D., 1995. Cavitation erosion of NiTi explosively welded to steel. Wear 181–183, 80–85.

Sokolnikoff, I.S., 1983. Mathematical Theory of Elasticity. Kreger Publishing Company, Malabar, Florida.

Sun, Q.-P., Hwang, K.-C., 1993. Micromechanics modeling for the constitutive behavior of polycrystalline shape memory alloys. Journal of the Mechanics and Physics of Solids 41, 1–33.

Tabor, D., 1996. Indentation hardness: fifty years on—a personal view. Philosophical Magazine A 74, 1207–1212.

Tunvisut, K., O'Dowd, N.P., Busso, E.P., 2001. Use of scaling functions to determine mechanical properties of thin coatings from microindenation tests. International Journal of Solids and Structures 38, 335–351.

Yan, W., 2006. Theoretical investigation of wear-resistance mechanism of superelastic shape memory alloy NiTi. Materials Science and Engineering A, in press.

Yan, W., Sun, Q.-P., Hwang, K.-C., 1998. A generalized micromechanics constitutive theory of single crystal with thermoelastic martensitic transformation. Science in China (Series A) 41, 878–886.

Yan, W., Wang, C.H., Zhang, X.P., Mai, Y.-W., 2003. Theoretical modelling of the effect of plasticity on reverse transformation in superelastic shape memory alloys. Materials Science and Engineering A 354, 146–157.

Yan, W., Sun, Q., Feng, X.-Q., Qian, L., 2006. Determination of transformation stresses of shape memory alloys—a method based on spherical indentation. Applied Physics Letters, in press.

Zarudi, I., Zhang, L.C., Swain, M.V., 2003. Behavior of monocrystalline silicon under cyclic microindentations with a spherical indenter. Applied Physics Letters 82, 1027–1029.